LETTER

doi:10.1038/nature13539

Widespread mixing and burial of Earth's Hadean crust by asteroid impacts

S. Marchi[1], W. F. Bottke[1], L. T. Elkins-Tanton[2]†, M. Bierhaus[3], K. Wuennemann[3], A. Morbidelli[4] & D. A. Kring[5]

The history of the Hadean Earth (~4.0–4.5 billion years ago) is poorly understood because few known rocks are older than ~3.8 billion years old[1]. The main constraints from this era come from ancient submillimetre zircon grains[2,3]. Some of these zircons date back to ~4.4 billion years ago when the Moon, and presumably the Earth, was being pummelled by an enormous flux of extraterrestrial bodies[4]. The magnitude and exact timing of these early terrestrial impacts, and their effects on crustal growth and evolution, are unknown. Here we provide a new bombardment model of the Hadean Earth that has been calibrated using existing lunar[4] and terrestrial data[5]. We find that the surface of the Hadean Earth was widely reprocessed by impacts through mixing and burial by impact-generated melt. This model may explain the age distribution of Hadean zircons and the absence of early terrestrial rocks. Existing oceans would have repeatedly boiled away into steam atmospheres as a result of large collisions as late as about 4 billion years ago.

Terrestrial planet formation models indicate the Earth went through a sequence of major growth phases: accretion of planetesimals and planetary embryos over many tens of millions of years (see, for example, ref. 6), culminating in a final giant impact that led to the formation of our Moon (see, for example, ref. 7). This was followed by the late accretion of leftover planetesimals that probably contributed less than 0.5% of the Earth's present-day mass[5]. Although the role of late accretion impacts on the Hadean Earth has long been discussed (for example, in ref. 8), the precise nature of the impactor flux during late accretion is elusive. Estimates from the abundance of highly siderophile elements (HSEs, such as Re, Au, Os and Ru) in mantle-derived peridotites indicate that $\sim(0.7–3.0)\times10^{22}$ kg of material with broad chondritic composition was added to the Earth[5], probably during the late accretion phase (see Methods).

An additional constraint on this flux comes from the ratio of HSEs found in the mantles of the Earth and Moon. Studies of terrestrial and lunar samples suggest that the ratio of the mass of broadly chondritic material accreted by the Earth and the Moon is probably $\gtrsim$700:1 (refs 9, 10). By modelling the impactor flux on both worlds, it has been argued[10] that this ratio was a reasonable outcome of stochastic accretion, with most HSEs added to the Earth by massive impactors that were statistically unlikely to strike the smaller Moon. This scenario was recently found to be broadly consistent with the current generation of models of terrestrial planet formation[11].

Here we assess the early Earth's impact history by rescaling a recent estimate of the lunar impact flux[4] to Earth. The advantages of this approach are numerous. First, the Moon provides a much clearer record of the early impact history of the Earth–Moon system[8]. Moreover, the lunar cratering record provides an absolute impactor flux that is independent of assumptions made by terrestrial planet formation models. The rescaling was done transforming lunar craters into a projectile flux, with the flux used to estimate the number of terrestrial impactors taking place in intervals of 25 Myr between 3.5 and 4.5 Gyr ago (see Methods). For the purpose of our work we assume that the Moon-forming impact was at

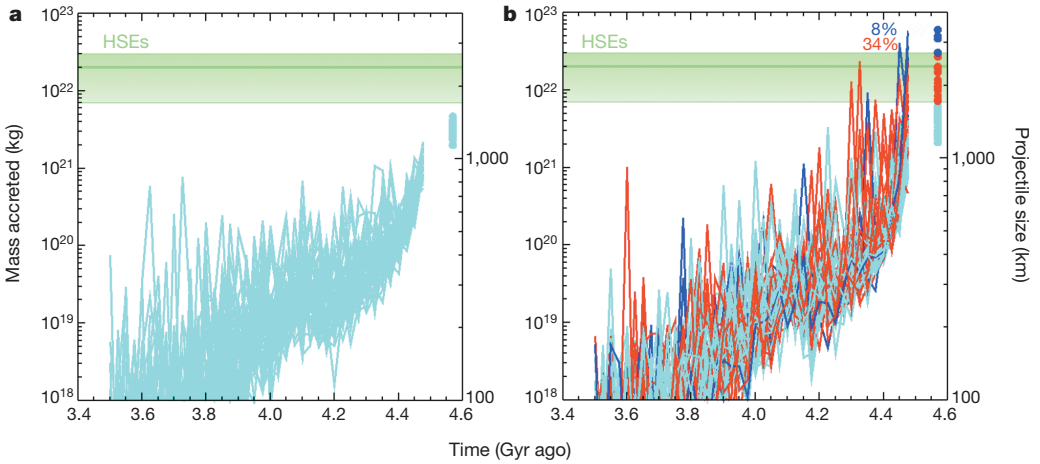

Figure 1 | Mass accreted by the Earth during the late accretion phase. **a**, Cyan curves show 50 representative Monte Carlo simulations corresponding to the main-belt size–frequency distribution truncated at Ceres (see Extended Data Fig. 1). Each data point indicates the total mass (left *y* axis) and equivalent diameter (right *y* axis) accreted in that time bin (of 25 Myr each). The cumulative accreted mass (or equivalent size) in the period 3.5–4.5 Gyr ago is indicated by the dots at the right of the panel. We assumed a projectile density of 3,000 kg m^{-3}. The horizontal green lines mark the lower, most probable and upper limits for the accreted mass as inferred from HSEs[5]. **b**, As in **a**, but for an impactor size–frequency distribution extrapolated at 4,000 km before 4.15 Gyr ago (see Extended Data Fig. 1). Simulations that deliver a mass within the HSEs range are in red; those in excess of the maximum limit are in blue (the corresponding percentages of simulations are indicated). These simulations were retained for further analyses.

[1]Southwest Research Institute, Boulder, Colorado 80302, USA. [2]Carnegie Institution for Science, Washington DC 20015, USA. [3]Museum für Naturkunde, Berlin 10115, Germany. [4]Observatoire de la Côte d'Azur, Nice 06304, France. [5]Universities Space Research Association, Lunar and Planetary Institute, Houston, Texas 77058, USA. †Present address: School of Earth and Space Exploration, Arizona State University, Tempe, Arizona 85287, USA.

~4.5 Gyr ago, but our results are insensitive to the exact timing. The sizes of the projectiles were randomly drawn from an assumed impactor size–frequency distribution (SFD) with a shape similar to that of large main-belt asteroids. The cut-off of this population was varied for different time intervals. Impactors striking after ~4.15 Gyr ago, the putative starting time of the late heavy bombardment (LHB[4,12–14]) were given a maximum cut-off of 1,000 km, roughly corresponding to the largest present-day asteroid Ceres. The impactor SFD before ~4.15 Gyr ago is assumed to have larger left-over planetesimals. We assumed a similar impactor SFD with a cut-off threshold at 4,000 km, which was extrapolated from the SFD of inner and central main-belt asteroids ranging between a few hundred kilometres to 1,000 km (see Methods and Extended Data Figs 1 and 2).

Using a Monte Carlo code, we repeated this procedure ~5,000 times to address the stochastic variability intrinsic to late accretion projectiles, and computed the accreted mass (Fig. 1). A key result is that, for the case of impactor SFD cut-off at 1,000 km, the total delivered mass is always below the range expected from HSEs (Fig. 1a), whereas a significant fraction of simulations (~30%) fall in this range when the cut-off is at 4,000 km before 4.15 Gyr ago (Fig. 1b). We assumed that all projectiles and their HSEs were fully accreted into the silicate Earth. Although the latter assumption is probably true for small projectiles that disintegrate in the impact event, larger objects may not deliver their HSEs efficiently to the mantle in all circumstances. Assuming that up to 50% of the cores of planetesimals ≥2,000 km may be lost (see Methods), we compute that the corresponding total percentage of successful simulations may be as high as ~40%. These results elucidate several important features of late accretion. The bulk of the mass (99% and 90%) is delivered by ~17 ± 5 and ~6 ± 3 largest projectiles, respectively, and the largest impactors can exceed ~3,000 km. This is therefore a highly stochastic regime, in which a few projectiles dominate the budget of HSEs delivered to Earth, in agreement with previous findings[10]. Moreover, by tracking the timing of the impacts, we also find that most of the mass is typically accreted over a significant fraction of the Hadean (~4.2–4.5 Gyr

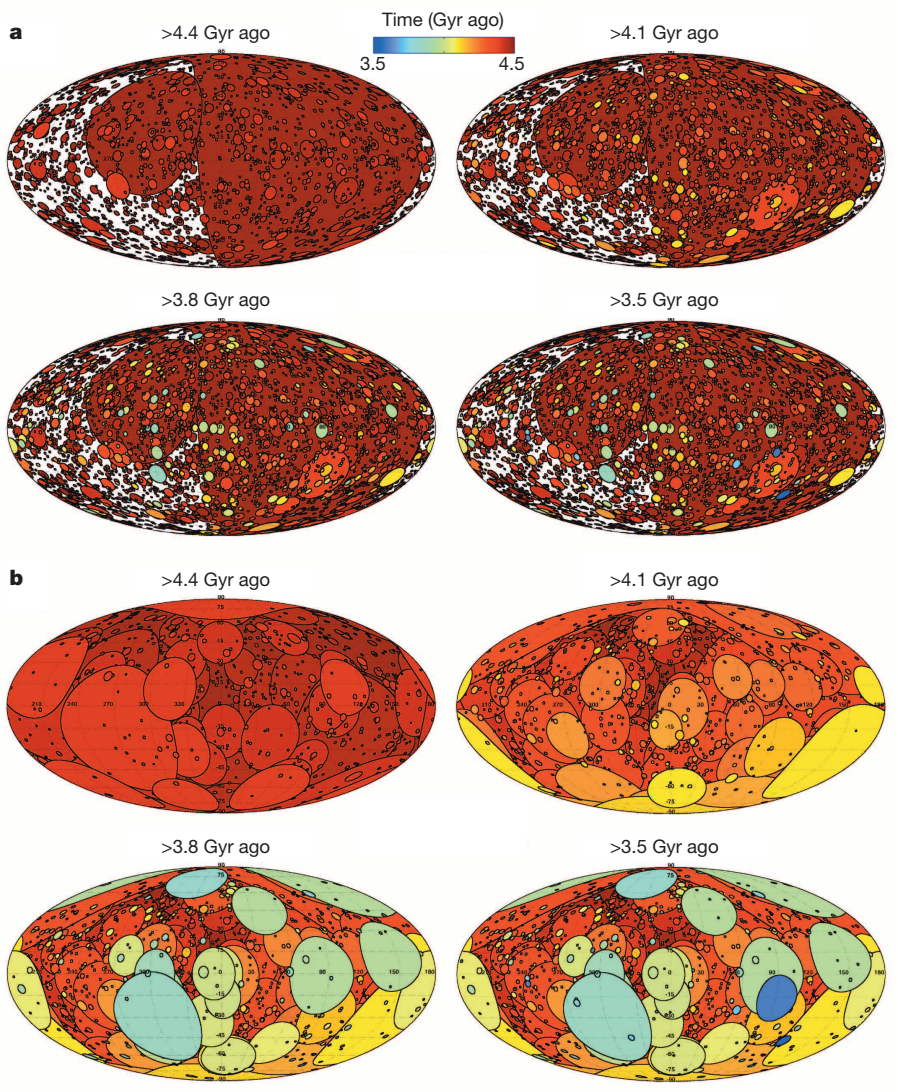

Figure 2 | Spatial distribution and sizes of craters formed on the early Earth. **a**, Mollweide projections of the cumulative record of craters at four different times. Each circle indicates the final crater size estimated from the transient cavity size from our simulations and a conservative estimate for the transient-to-final crater size scaling (see Methods). The maps do not show ejecta blankets and melt extrusion on the surface, which can greatly expand the effects of cratering; they also do not account for a hotter early geotherm, which would also result in larger crater sizes (see Methods). The colour coding indicates the time of impact. The smallest projectiles considered have a diameter of 15 km. We assumed an impact velocity of ~16 and ~25 km s^{-1} before and after 4.15 Gyr ago (see Methods), respectively, and a most likely impact angle of 45°. **b**, As in **a**, but including melt extrusion on the surface as discussed in the text.

ago), suggesting that the early Hadean silicate Earth could have had a substantially different budget of HSEs and trace elements compared with the current Earth (see Methods). Note also that less than 0.5% of the simulations deliver more than 1% of an Earth mass.

Our terrestrial bombardment model also sheds light on the role of impacts on the geological evolution of the Hadean Earth, with particular emphasis on mixing, burial and melting of the uppermost layers. To model these effects quantitatively, we performed a suite of impact simulations with the Simplified Arbitrary Lagrangian Eulerian shock-physics code (iSALE[15]), and computed the resulting excavation cavity size, excavation volume and depth, and the volume of target melt. We varied the target temperatures and considered impactor diameters ranging from 15 to 4,000 km with a range of impact velocities (see Methods).

A key process is the impact-generated mixing as a result of the excavation and collapse of large transient cavities in the lithosphere. We found that before ~4.4 Gyr ago up to 60–70% of the Earth's surface was reworked to a median depth of 20 km (Fig. 2a). Thus, our model predicts prolonged crustal reworking and mixing of various components, as inferred from recent Pb–Hf isotope systematics of Hadean zircons[16].

Melting of the target is an additional important process. We computed the melt produced by shock pressure, using both analytical estimates[17,18] and iSALE simulations. Our simulations agree well with analytical estimates for impactor sizes below 100 km, but deviate significantly for larger impactors (Fig. 3a) (see Methods and Extended Data Figs 3 and 4). Both methods neglect impact-induced decompression and subsequent adiabatic melting of rising material in the mantle, which increase the total volume of melt. These processes have been quantitatively modelled for impactor diameters smaller than 100 km (ref. 19), and here we use their predictions for an impactor 100 km in diameter and then extrapolate their results to larger projectiles (Fig. 3a). Note that the melt volume is a lower limit for large projectiles that are expected to induce major mantle perturbations, resulting in voluminous adiabatic melting[20]. Computed melt volumes greatly exceed the volumes of current flood basaltic provinces[19]. Some fraction of the mantle melt will erupt; through isostatic adjustment, melt may be expelled from the shallowing crater onto the planetary crust[17]. Melt spreading is also aided by the dynamics of cavity collapse in a hotter crust[21], such as that envisioned to have occurred during the Hadean[22]. Assuming that the impact-generated melt flows on the surface, we used the estimated melt volumes to calculate that the corresponding diameter of a spherical cap with a thickness of 3 km (comparable to large terrestrial igneous provinces) is ~20–30-fold that of the impactor diameters (see Fig. 3b). As a result of melt spreading, lithologies previously exposed at the surface are buried over large areas.

The effects of melt burial due to impacts are shown in Fig. 2b. The cumulative fraction of Earth's surface buried by impact-generated melt is 70–100% since 4.15 Gyr ago, and it increases to 400–600% during the period 4.15–4.5 Gyr ago. These findings do not preclude the possibility of having large unaffected surface areas at any given time step (see Fig. 2b, Extended Data Fig. 5), a condition required for liquid water to be stable at the surface as indicated by $\delta^{18}O$ measurements in Hadean zircons[23,24].

Additional constraints on the terrestrial bombardment flux may come from trace elements entrapped in Hadean zircons. Their rare-earth elements, U–Pb and Pb–Hf ages and Lu/Hf ratios point to significant mixing of mafic and felsic reservoirs (see, for example, ref. 16). This mixing is sometimes attributed to volcanism or subduction[3,16,22], in which weathered upper crustal reservoirs are buried at depth. Once buried, the different components melt, and the resulting magma can then crystallize Hadean zircons[3]. It is unclear, however, whether these processes can readily explain the observed age distribution of Hadean zircons, which is characterized by a well-defined peak at 4.1–4.2 Gyr ago and a lack of ages older than ~4.4 Gyr (ref. 2). Moreover, it is unresolved whether the lack of ultra-ancient zircons implies that the right conditions for zircon formation were not met during this time, or whether zircons older than ~4.4 Gyr did not survive subsequent evolution.

Our model shows that substantial burial could be achieved by impact-generated melt. Assuming that burial is required to make Hadean zircons[3,16,22], we investigated whether the burial by impact-generated melt could explain the Hadean zircons age distribution. In our Monte Carlo code, each simulated impact was assumed to bury surface lithologies within a threshold distance proportional to the projectile diameter d multiplied by a factor f ($\sim fd$). This process results in increased crustal temperatures over a large annulus around the impact site, possibly leading to eutectic melting of buried wet crustal material, in agreement with the observation that many of the Hadean zircons probably crystallized

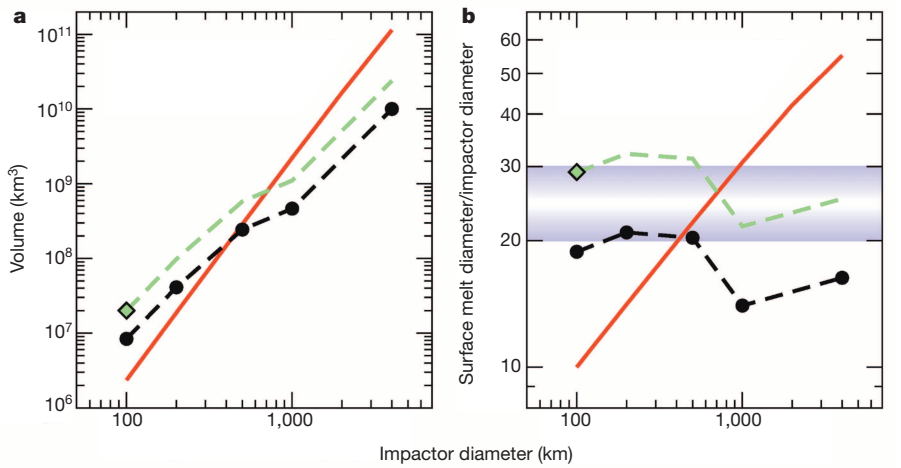

Figure 3 | Melt production by large impacts on the Earth. **a**, Impact-shock melt volume from analytical estimates[18] (red line), and impact-generated melt volume (including shock and decompression melting) for impacts simulated with iSALE (black dots). These simulations assumed a planar target, a lithospheric thickness of 125 km, a mantle potential temperature of 1,400 °C, an impact velocity of 12.7 km s^{-1} (corresponding to 18 km s^{-1} for an impact angle of 45°). The mantle potential temperature of the Hadean Earth may have been hotter than assumed here by ~200 °C (see Methods and Extended Data Table 1). We also ran simulations for a mantle potential temperature of 1,600 °C and found that the melt volume increased by 75% (see Methods). The green diamond represents the total melt volume (including decompression and adiabatic melting) from ref. 19 for a crater 800 km in diameter (corresponding to an impactor of 100 km for the assumed impact conditions) and a mantle potential temperature of 1,450 °C. The latter data point is 2.3-fold higher than our data point. Assuming that a similar scaling holds for larger projectiles, we obtain the green curve. The curves neglect adiabatic melting and therefore provide a lower limit for the total impact-generated melt. **b**, Ratio of surface melt diameter (for a thickness of 3 km) to impactor diameter (f). The horizontal grey area indicates f = 20–30, as discussed in the text. Symbols as in **a**.

from wet eutectic melts[3]. The increase in crustal temperatures is caused by the hotter geotherm of the buried material produced by melt above and possible thinning from the bottom, the rise of mantle melts into the fractured and tectonized lithosphere close to the crater's rims[19,25], and possibly also by dripping crustal diapirs originating from the thick surface melt layer at larger radial distances[26].

We find that for $f \approx 20$–30 for impactor diameters larger than 100 km, as predicted by our simulations, the resulting surface age distribution matches well the Hadean zircon age distribution (see Fig. 4). In contrast, simulations having $f \lesssim 20$ or $f \gtrsim 40$ fail to reproduce the data (see Methods). This fit, if not a coincidence, tells us that large projectiles were capable of making zircons and resetting pre-existing ones over regions well beyond their computed crater rims, in agreement with our estimates of impact-generated melt (Fig. 3).

Several observations may be explained by consequences of the proposed mechanism for Hadean zircons formation. First, given that large impactors could have struck at relatively late times (for example the expected surge of projectiles at 4.15 Gyr ago via the LHB), zircon production through these impact-generated processes could have occurred for many hundreds of millions of years, as observed[2,27]. Attrition among the oldest zircons was pronounced, because they were subject to high temperatures near numerous impact locations[28], burial at depth by melt and ejecta, and redistribution to the upper crust. Most were reset or destroyed. Consequently, our model predicts that the paucity of zircons older than 4.4 Gyr is expected from collisional processes. Moreover, the formation of Hadean zircons at depth in large annuli around major impacts provides a ready explanation for their lack of clear signs of impact shock[2,27] that are commonly observed among younger zircons. Another attractive aspect of our model is that it explains the mixing of the protoliths from which Hadean zircons crystallized, as inferred from the Hf-isotope record[29]. Finally, the volume of the buried lithologies at any time step is about an order of magnitude higher than the fraction of the crust melted by small impacts, indicating that the zircon crystallization from impact melts was negligible (see Methods), in agreement with the low crystallization temperatures observed in Hadean zircon [30,31].

We argue that the peak of Hadean zircon ages at 4.1–4.2 Gyr reflects the onset of the LHB, as suggested by meteorite Ar–Ar shock degassing ages and other data[13,14]. Indeed, we find that a scenario with an LHB spike at significant younger ages, say 3.9 Gyr, is inconsistent with Hadean zircon age distributions. A similar conclusion is reached for a steadily declining bombardment (no LHB) scaled to match the abundance of lunar HSEs (see Methods). Therefore, LHB-era impactors provide a natural explanation for the clustering of Hadean zircon ages that would otherwise require *ad hoc* endogenic conditions (for example increased subduction or volcanism rates).

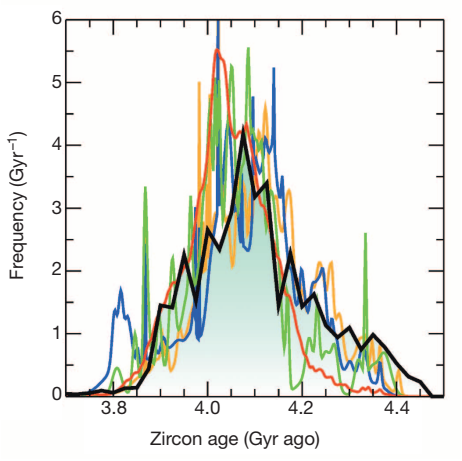

Figure 4 | Detrital Hadean zircon ages compared with the computed distribution of impact-generated ages. Zircon ages (coloured curves correspond to different data sets: orange, ^{207}Pb–^{206}Pb ages[2]; blue, U–Pb ages[29]; green, ^{207}Pb–^{206}Pb ages[16]; red, U–Pb ages[32]) show a distinct peak at ~4.1–4.2 Gyr ago. In agreement with our iSALE simulations, the distribution of impact-generated ages (black line, shaded area) is computed for $f = 30$ for projectiles larger than 100 km and $f = 9$ for projectiles smaller than 100 km, and is an average of 50 successful Monte Carlo simulations (Fig. 1). All distributions are normalized to unit area.

The new picture of the Hadean Earth emerging from our work has important implications for its habitability. Before ~4 Gyr ago, no substantial large region of the Earth's surface could have survived untouched by impacts and associated outcomes. Large impacts had particularly severe effects on extant ecosystems. We find that the Hadean was plausibly characterized by one to four impactors larger than 1,000 km capable of global sterilization[8], and by three to seven impactors larger than 500 km capable of global ocean vaporization[8]. The median time for the latest impactor larger than 500 km to hit the Earth was ~4.3 Gyr ago. In ~10% of the simulations, this could be as recently as ~4 Gyr ago (Extended Data Fig. 6), depending on various assumptions. Thus, life emerging during the Hadean was probably resistant to high temperatures and was capable of spreading from the stable niches that existed at that time.

Online Content Methods, along with any additional Extended Data display items and Source Data, are available in the online version of the paper; references unique to these sections appear only in the online paper.

Received 4 March; accepted 23 May 2014.

1. Kamber, B. S., Moorbath, S. & Whitehouse, M. J. The oldest rocks on Earth: time constraints and geological controversies. *Geol. Soc. Lond. Spec. Publ.* **190,** 177–203 (2001).
2. Cavosie, A. J., Valley, J. W. & Wilde, S. A. In *World's Oldest Rocks* (ed. Condie, K.) 111–129 (Developments in Precambrian Geology vol. 15, Elsevier, 2007).
3. Harrison, T. M. The Hadean Crust: evidence from >4 Ga zircons. *Annu. Rev. Earth Planet. Sci.* **37,** 479–505 (2009).
4. Morbidelli, A., Marchi, S., Bottke, W. F. & Kring, D. A. A sawtooth-like timeline for the first billion years of lunar bombardment. *Earth Planet. Sci. Lett.* **355–356,** 144–151 (2012).
5. Walker, R. J. Highly siderophile elements in the Earth, Moon and Mars: update and implications for planetary accretion and differentiation. *Chem. Erde* **69,** 101–125 (2009).
6. Chambers, J. E. Planetary accretion in the inner Solar System. *Earth Planet. Sci. Lett.* **223,** 241–252 (2004).
7. Canup, R. M. Dynamics of lunar formation. *Annu. Rev. Astron. Astrophys.* **42,** 441–475 (2004).
8. Sleep, N. H., Zahnle, K. J., Kasting, J. F. & Morowitz, H. J. Annihilation of ecosystems by large asteroid impacts on the early earth. *Nature* **342,** 139–142 (1989).
9. Day, J. M. D., Pearson, D. G. & Taylor, L. A. Highly siderophile element constraints on accretion and differentiation of the Earth–Moon system. *Science* **315,** 217–219 (2007).
10. Bottke, W. F., Walker, R. J., Day, J. M. D., Nesvorny, D. & Elkins-Tanton, L. Stochastic late accretion to Earth, the Moon, and Mars. *Science* **330,** 1527–1530 (2010).
11. Raymond, S. N., Schlichting, H. E., Hersant, F. & Selsis, F. Dynamical and collisional constraints on a stochastic late veneer on the terrestrial planets. *Icarus* **226,** 671–681 (2013).
12. Marchi, S. *et al.* Global resurfacing of Mercury 4.0–4.1 billion years ago by heavy bombardment and volcanism. *Nature* **499,** 59–61 (2013a).
13. Bottke, W. F. *et al.* An Archaean heavy bombardment from a destabilized extension of the asteroid belt. *Nature* **485,** 78–81 (2012).
14. Marchi, S. *et al.* High-velocity collisions from the lunar cataclysm recorded in asteroidal meteorites. *Nature Geosci.* **6,** 303–307 (2013b).
15. Wünnemann, K., Collins, G. S. & Melosh, H. J. A strain-based porosity model for the use in hydro code simulations of impact and implications for transient crater growth in porous targets. *Icarus* **180,** 514–527 (2006).
16. Kemp, A. I. S. *et al.* Hadean crustal evolution revisited: New constraints from Pb-Hf isotope systematics of the Jack Hills zircons. *Earth Planet. Sci. Lett.* **296,** 45–56 (2010).
17. Tonks, W. B. & Melosh, H. J. Magma ocean formation due to giant impacts. *J. Geophys. Res.* **98,** 5319–5333 (1993).
18. Reese, C. C. & Solomatov, V. S. Fluid dynamics of local martian magma oceans. *Icarus* **184,** 102–120 (2006).
19. Elkins-Tanton, L. T. & Hager, B. H. Giant meteoroid impacts can cause volcanism. *Earth Planet. Sci. Lett.* **239,** 219–232 (2005).
20. Watters, W. A., Zuber, M. T. & Hager, B. H. Thermal perturbations caused by large impacts and consequences for mantle convection. *J. Geophys. Res. Planets* **114,** E02001 (2009).
21. Potter, R. W. K., Collins, G. S., Kiefer, W. S., McGovern, P. J. & Kring, D. A. Constraining the size of the South Pole–Aitken basin impact. *Icarus* **220,** 730–743 (2012).
22. Kamber, B. S., Whitehouse, M. J., Bolhar, R. & Moorbath, S. Volcanic resurfacing and the early terrestrial crust: Zircon U-Pb and REE constraints from the Isua

Greenstone Belt, southern West Greenland. *Earth Planet. Sci. Lett.* **240,** 276–290 (2005).
23. Mojzsis, S. J., Harrison, T. M. & Pidgeon, R. T. Oxygen-isotope evidence from ancient zircons for liquid water at the Earth's surface 4,300 Myr ago. *Nature* **409,** 178–181 (2001).
24. Wilde, S. A., Valley, J. W., Peck, W. H. & Graham, C. M. Evidence from detrital zircons for the existence of continental crust and oceans on the Earth 4.4 Gyr ago. *Nature* **409,** 175–178 (2001).
25. Wichman, R. W. & Schultz, P. H. Sequence and mechanisms of deformation around the Hellas and Isidis impact basins on Mars. *J. Geophys. Res.* **94,** 17333–17357 (1989).
26. Bedard, J. H. A catalytic delamination-driven model for coupled genesis of Archaean crust and sub-continental lithospheric mantle. *Geochim. Cosmochim. Acta* **70,** 1188–1214 (2006).
27. Cavosie, A. J., Valley, J. W. & Wilde, S. A. Magmatic $\delta^{18}O$ in 4400–3900 Ma detrital zircons: a record of the alteration and recycling of crust in the Early Archean. *Earth Planet. Sci. Lett.* **235,** 663–681 (2005).
28. Abramov, O., Kring, D. A. & Mojzsis, S. J. The impact environment of the Hadean Earth. *Chemie Erde Geochem.* **73,** 227–248 (2013).
29. Griffin, W. L. *et al.* The world turns over: Hadean–Archean crust–mantle evolution. *Lithos* **189,** 2–15 (2014).
30. Watson, E. B. & Harrison, T. M. Zircon thermometer reveals minimum melting conditions on earliest Earth. *Science* **308,** 841–844 (2005).
31. Darling, J., Storey, C. & Hawkesworth, C. Impact melt sheet zircons and their implications for the Hadean crust. *Geochim. Cosmochim. Acta* **73** (Suppl.), 927–930 (2009).
32. Holden, P., Lanc, P. & Ireland, T. *et al.* Mass-spectrometric mining of Hadean zircons by automated SHRIMP multi-collector and single-collector U/Pb zircon age dating: the first 100,000 grains. *Int. J. Mass Spectrom.* **286,** 53–63 (2009).

Acknowledgements We thank H. J. Melosh, S. J. Mojzsis, T. M. Harrison, A. J. Cavosie, A. I. S. Kemp, W. L. Griffin, M. M. Wielicki, R. J. Walker, E. B. Watson, P. Holden, O. Abramov, R. M. Canup, H. F. Levison, D. Nesvorny, O. Nebel, N. H. Sleep and N. Arndt for comments and criticisms that helped to shape the current paper. We gratefully acknowledge the developers of iSALE-2D/3D (www.isale-code.de). S.M., W.F.B. and D.A.K. received support from the NASA Solar System Exploration Research Virtual Institute grant no. NNA14AB03A and NNA14AB07A; K.W. and M.B. were supported by the Helmholtz-Gemeinschaft Deutscher Forschungszentren e.V. Alliance 'Planetary Evolution and Life'. A.M. was supported by the European Research Council Advanced Grant 'ACCRETE' (contract number 290568).

Author Contributions S.M. conceived the paper, built the Monte Carlo code and executed the simulations. W.F.B. and A.M. contributed to calibration and testing of the code, and to performing the fit of zircon age distributions. M.B. and K.W. executed iSALE impact simulations and processed the results. L.T.E.T. performed the geophysical interpretation of the output of the simulations. D.A.K. interpreted the melt volume. All authors contributed to the discussion of the results and their implications and to the crafting of the manuscript.

Author Information Reprints and permissions information is available at www.nature.com/reprints. The authors declare no competing financial interests. Readers are welcome to comment on the online version of the paper. Correspondence and requests for materials should be addressed to S.M. (marchi@boulder.swri.edu).

METHODS

Impactor size–frequency distribution and flux. The SFD of bodies colliding with the early Earth cannot be directly constrained because subsequent geological evolution has erased the signatures of those impacts. Instead, we turn to very old cratered terrains found on the Moon, Mars and Mercury. The crater SFDs observed on those terrains has been used to constrain the shape of the impactor SFD in ancient times. The earliest visible populations of craters have a characteristic SFD resembling that of the current main asteroid belt[12,33–36]. In this work we assume that a similarly shaped impactor SFD was striking the early Earth. Although it is natural to assume that the Earth and Moon have been exposed to the same impactor flux, a critical aspect of work concerns the impactor SFD at large sizes. In fact, the larger geometrical cross-section of the Earth than that of the Moon may allow larger projectiles to hit the Earth than the Moon. For comparison, the largest confirmed impact structure in the inner Solar System—the ~2,500–km South Pole–Aitken basin on the Moon—was produced by a projectile ~170 km across[21]. It is possible that larger objects struck the early Earth, in particular if the shape of the impactor SFD was shallow for large objects (see, for example, ref. 10). Therefore the impactor SFDs derived from crater populations observed on the terrestrial planets needs to be extrapolated to larger sizes if they are to be applied to the Earth. For the reasons discussed above, we considered a main-belt-like SFD up to ~1,000 km (Ceres), and we also considered an extension of the main-belt SFD up to 4,000 km (see the text and Extended Data Fig. 1 for further details).

The results of our work are not sensitive to the fine details of the shape of the impactor SFD. The more important issue is that the population of left-over planetesimals had large enough impactors (diameter >1,000 km) to allow it to reproduce the abundance of terrestrial HSEs. Here we consider a cut-off of 4,000-km and 1,000-km projectiles for impactors striking before and after 4.15 Gyr ago, respectively. The number of large objects in the population can conceivably be constrained by the largest lunar basin, provided that these impacts took place after the formation of the Moon's crust. Our modelling work indicates that the Earth was hit by 25–45 impactors larger than 200 km. Assuming a Earth-to-lunar scaling of ~20:1 (ref. 13), we obtain one or two South Pole–Aitken-forming impactors hitting the Moon. This is consistent with the lunar basin record and the lunar HSEs. We also estimate that an average of five impactors larger than 500 km hit the Earth. This translates into a ~70% (= 1 − 6/20) probability that the Moon escapes these impacts. These numbers provide a sanity check that our assumed impactor SFD is compatible with available constraints.

Note also that in an alternative scenario for the origin of the HSEs found within the mantles of the Earth and Moon[37], it has been argued that a thin, dynamically cold disk of small bodies spread across the terrestrial planet region would allow the Earth to accrete much more mass than the Moon. This scenario requires that a very thin disk be maintained during the planet formation era until the giant impact that made the Moon take place—probably many tens of millions of years to perhaps 100 Myr after Ca, Al-rich inclusions formation. It is unclear to us how this disk avoided dynamical excitation from planetary perturbations for this long interval (well after the solar nebula had dissipated). Beyond this, concerning HSEs on or in the Moon, this scenario would produce high enrichment in HSEs in the lunar crust (which is not observed) and it does not explain how the HSEs within the small bodies would breach the crust to reach the Moon's mantle. There is also no explanation provided of how this scenario would produce the crater SFDs found on ancient lunar terrains[35].

Concerning the terrestrial impact rate, we considered several scenarios. The nominal model assumes the so-called lunar sawtooth bombardment profile for the Moon[4] extrapolated to the Earth. For this, we took the lunar impactor flux (as derived from the observed number of craters as a function of time), defocused it for the lunar gravitational field and Earth's gravitational field at the current lunar orbit, and then applied the Earth's gravitational focusing. More specifically, the crater size–frequency distribution on ancient lunar terrains has been converted into projectiles assuming first, a crater-to-projectile size scaling law for hard-rock[38]; second, a lunar impact velocity of 11 km s^{-1} for the period between 4.15 and 4.5 Gyr ago; and third, a lunar impact velocity of 22 km s^{-1} for the period between 3.5 and 4.15 Gyr ago. The factor of ~2 increase in the impact velocity comes from observations of lunar crater populations[35] and is in agreement with dynamical estimates of terrestrial planet accretion[11] and how projectiles in the inner Solar System may have reacted to late migration of the giant planets[13]. The corresponding terrestrial impact velocities are ~16 and ~25 km s^{-1}. The projectile flux and impact velocity were then rescaled to the Earth, assuming that impactors producing the oldest visible lunar craters were not affected by Earth's gravitational focusing. This approximation is valid for most of the Moon's orbital evolution except for the first few million years (ref. 39), which are not relevant to the work presented here. This procedure gives a flux scaling factor for the Earth and Moon of ~1.24 and ~1.90 (per unit surface), respectively, for the LHB and pre-LHB times for the assumed impact speed at infinity. As detailed in the text, our extrapolation is done by rescaling the lunar flux to the Earth. Here we assume that the LHB occurred at ~4.15 Gyr ago (the median value of the 4.1–4.2-Gyr interval of acceptable values, as concluded in refs 4, 13). The corresponding lunar flux curve is shown by the red line in Extended Data Fig. 2. We also considered the case of a narrow intense spike of LHB impacts at 3.9 Gyr ago, roughly corresponding to the scenario discussed in ref. 40 (cyan curve). Recent work has suggested that this LHB is unlikely to fit constraints[4,13,14,41]. However, this assumption is still adopted by some researchers. Both of our impact flux curves were obtained by requiring that the integral of the accreted mass on the Moon match the abundance of lunar HSEs inferred to exist in the Moon's mantle, appropriately corrected to take into account partial accretion[4]. Finally, for the sake of completeness, we also considered two scenarios that exclude the LHB. The first is a simple extrapolation of the nominal case up to 4.5 Gyr ago (black curve). Note that here the total mass accreted by the Moon exceeds that predicted by the HSEs by a factor 3–4; therefore ref. 4 concluded that this scenario is unlikely. To compensate for this, we also considered a rescaled flux, reduced by a factor of one-third, to match the HSE constraint (green curve). All flux curves start at 4.5 Gyr ago, which is the assumed time for the formation of the Moon; however, our results are insensitive to the exact timing of Moon formation. We discuss how these curves compare with terrestrial zircon data in the following.

Terrestrial budget of HSEs. Terrestrial impactors may not be fully accreted with implication for the delivery of HSEs. For instance, this may be the case for large grazing projectiles[42]. In addition, projectiles larger than ~2,000 km may sequester mantle HSEs into Earth's core[43], whereas high-resolution smoothed-particle hydrodynamics simulations show that as much as ~50% of the core of a large differentiated impactor may plunge into the Earth's core (R. M. Canup, personal communication, August 2013). Thus, in scenarios involving collisions with projectiles larger than ~2,000 km the accreted mass would be higher than that estimated by HSEs (see Fig. 1).

Moreover, is it possible that some terrestrial HSEs predate the formation of the Moon? In canonical giant impact events that make the Moon[7], most of the Earth's mantle is molten or partly molten, thus facilitating the segregation of HSEs into the core. Recent models have pushed the giant collisions to higher energies with respect to the canonical models; therefore an efficient segregation of pre-giant impact HSEs is even more likely (R. M. Canup, personal communication, April 2014). Ref. 44 found that ε^{182}W (that is, the ratio of sample $^{182}W/^{184}W$ to the terrestrial standard value, in parts per 10^4) of the Moon is significantly different with respect to that of the Earth. This can be explained if an amount of tungsten with a broadly chondritic isotope ratio was delivered in chondritic proportions with the HSEs. This would suggest that HSEs were mostly accreted after the formation of the Moon.

Simulations of large terrestrial impacts with iSALE. Investigating the thermal effects of the early bombardment history on Earth implies a detailed quantitative understanding of the consequences of hypervelocity impacts of cosmic bodies of given mass, composition, velocity, and angle of incidence. Hydrocode modelling may serve as the most accurate approach with which to estimate crater size and the amount of shock wave-induced heating and melting of crustal and mantle rocks as the result of a collision. However, given the large number of collisions produced on the early Earth, it is impossible to model each impact event individually. A parameterization of the relationship between the size of an impact event (projectile mass m, diameter d, impact velocity v and impact angle α) and the resulting crater diameter D, depth h, volume V, excavation depth d_{ex}, excavation volume V_{ex} and melt volume V_{melt} is required. Existing scaling relationships (for example, refs 45–54) are based on laboratory and numerical experiments, analytical considerations and observations of the Earth's and lunar crater records. Whether these scaling relationships can be extrapolated to the size of impactors several hundred of kilometres in diameter as those that occurred in the early history of the Earth is questionable and requires further analysis and/or modifications of existing scaling laws to confirm their applicability to the given problem.

We used the hydrocode iSALE (see ref. 15 and references therein) to conduct a series of two-dimensional numerical models of impacts with projectile diameters d ranging from 1 to 1,000 km and impact velocities v of 8.5–17 km s^{-1} (a few runs for 4,000-km impactors were also performed). In all models the impactor is resolved by 50 cells per projectile radius, and we assume a dunitic composition with a density $\delta = 3{,}314\ kg\ m^{-3}$. We do not consider the impact angle α, which naturally can vary between 0° and 90°, with the most likely encounter at 45°, and modelled vertical impacts (90°) only on a cylindrical, axial-symmetric two-dimensional grid on a planar target surface. Both simplifications (vertical impacts and planar target surface) reduce the computational costs of an individual simulation significantly and thus permit detailed parameter studies based on a sufficient number of numerical models. To compensate for the lack of varying impact angles in our models we assume an impact velocity that corresponds to the vertical component of the velocity vector ($v_p = v \sin\alpha$), an often-used simplification to approximate oblique impacts by two-dimensional simulations[48,55,56] that was originally suggested in ref. 57.

In the baseline scenario, we assume a layered target composed of a lithosphere 125 km thick consisting of a 30-km granitic crust and a 95-km dunitic upper mantle. Within the lithosphere, heat is transported by conduction, giving rise to a relatively steep temperature gradient from 20 °C at the surface to 1,427 °C at the transition from the upper to the lower mantle (the asthenosphere; Extended Data Fig. 3). The temperature gradient in the asthenosphere is adiabatic according to the assumption that heat is transported by convection. At a depth of 2,930 km we consider an iron core with a constant temperature of 2,727 °C. Because we assume pure iron and neglect alloy composition, the solidus is relatively high and the core is in a solid state; however, the rheological properties of the core do not affect our models, because the craters in the biggest impact events under consideration do not reach as deep.

The thermodynamic behaviour of matter in our models is simulated by the ANEOS (Analytic Equation of State; ref. 58) for granite[53] and dunite[59]. ANEOS can only account for one phase transition; we therefore took into account the solid state transition expected to have the biggest effect on the total amount of melt production by shock heating. Because we do not consider latent heat of melting, our estimate of shock melting corresponds to an upper estimate (for further explanations see refs 53, 60, 61). The rheological model, the resistance of rocks against plastic deformation, is explained in detail in ref. 62. We do not account for temporary weakening of matter during crater formation by acoustic fluidization[63] as required to explain mid-size complex crater morphologies. All material properties and model parameters are listed in Extended Data Table 1. We also neglect the effects of target spherical symmetry, which are estimated to contribute less than ~20% to the volume of melt for the impactor sizes considered in our work[17]. Note that direct two-dimensional cylindrical iSALE simulations (equivalent to full three-dimensional simulations for head-on collisions) have shown that the target curvature is negligible for projectile-to-target size ratios up to ~0.2 (ref. 64), corresponding to a projectile of 2,500 km for the Earth, in agreement with analytical estimates[17]. This gives confidence in the validity of the analytical estimates. The analytically estimated error of ~20% for the largest projectiles is within the error of our model.

All models begin with the first contact between the projectile and the target (we neglect the presence of an atmosphere) and stop after the collapse of the transient crater. Our models include the structural uplift of matter but do not last until all material is settled and the final crater is reached. Primarily our simulations aim at the determination of crater size, excavation depth and the melt that is generated by the impact event.

Previous studies aimed at the computation of impact melt volumes usually considered shock-induced melting only. Melting of rocks during impact is the result of shock-wave compression and subsequent release. Shock compression is an irreversible process in which plastic work is done on the target material that remains in the rock as heat after subsequent isentropic release and can raise the temperature of the target above the melt temperature. To quantify the amount of impact-generated melt it is necessary to determine the volume of material that experiences a peak shock pressure in excess of the material's critical shock pressure for melting (P_c). The critical shock pressure for melting (or the corresponding entropy) for granite and dunite is a material property that can be measured by shock experiments (see, for example, ref. 65) and serves as an input parameter for ANEOS[53]. Because the petrographical composition for a given rock type, such as dunite, may vary, the stated P_c values found in the literature range from ~91 to ~156 GPa depending on whether pure fosterite or peridotite composition and incipient or complete melting are considered, respectively. Extended Data Fig. 4a shows the impact melt production determined by hydrocode simulations for impacts on layered targets (granite and dunite; see above) in comparison with scaling relationships proposed by refs 17, 18, 51. Extended Data Fig. 4b shows the dependence of melt production on impact velocity. The melt volume is determined in our hydrocode simulations by Lagrangian tracer particles that experience shock pressures in excess of P_c. Each tracer represents the amount of matter in the computational cell where it was initially located in (see, for instance, ref. 61). Apparently, the melt volume varies at most by a factor of two depending on the chosen P_c (91 or 156 GPa, respectively), which we consider to be insignificant for the present study. Thus, a more accurate approach considering partial melting if the post-shock temperature is between solidus and liquidus as proposed in ref. 66 was not included in this study. The much lower P_c for granite (46 GPa for incipient melting and 56 GPa for complete melting[53]) raises the total amount of melt for impactors <100 km in diameter more significantly; however, for very large impactors (>100 km in diameter) the total amount of melt is dominated by mantle material, and the contribution of crustal material is negligible.

The critical pressure method for the quantification of impact melt production is in good agreement with estimates of the observed melt volumes at terrestrial impact craters[49], but it may not provide accurate estimates for very large impactors several hundred kilometres in diameter penetrating deep into Earth's mantle, for two reasons. First, with increasing depth, where material experiences shock compression the pre-impact temperature and lithostatic pressure become important. The initial temperature of the rock affects the critical melt pressure P_c: preheated rock tends to show shock-metamorphic effects including melting at lower shock pressures than rocks at normal surface temperature[67,68]. Second, at a depth approximately larger than the transition from the lithosphere to the asthenosphere, rocks may not melt at all because the lithostatic pressure raises the solidus above the shock-induced temperature increase. Contrarily, structural uplift of originally deep-seated material as a result of the gravity-driven collapse of the transient crater may give rise to decompression melting. However, the effect of decompression melting has been estimated to be small in comparison with shock-induced melting for impactors 20 km in diameter[69], but may well be important for very large impactors and steep geotherms[66].

To account for both effects (temperature increase with depth and unloading from the shock pressure to the lithostatic pressure at given depth) we used an alternative approach to determine the total amount of impact-generated melt. We simply record through all computational time steps in our hydrocode simulations whether the temperature of a tracer is in excess of the solidus temperature as a function of pressure for the given location (depth) and mark it as molten. For small impactors (a few kilometres in diameter) this approach provides the same results as the P_c method (see Extended Data Fig. 4). With increasing projectile diameter the melt volume deviates from the scaling lines (open circles) according to the critical pressure method, and slightly increased melt volumes occur (50–100 km projectile diameter; note the small variation at 25 km diameter resulting from the change from a granitic to a dunitic melt composition). For larger impactors (>100 km diameter) the melt volumes decrease below the expected trend according to a straight line on a double-logarithmic plot (power-law scaling). This is due to the fact that shock-heated material does not unload to pressures at which the post-shock temperature is in excess of the solidus temperature. The reason for this is the fact that the increase in solidus temperature with depth is steeper than the increase in adiabatic temperature in the lower mantle (Extended Data Fig. 3). Increasingly higher shock pressures are therefore required to raise the temperature above the solidus. In summary, the difference between iSALE simulations and the analytical estimates can be understood by accounting for the different assumptions used for each case. For example, using projectile diameters in the range ~100–1,000 km, our simulations predict more melt than analytical estimates do[17,18], because the code accounts for decompression melting. In contrast, for projectiles larger than 1,000 km, iSALE finds less melt than our analytical estimates[17,18] because the latter neglects the increase of the solidus temperature as a function of depth.

Our analytical scaling relationships for melt production and crater sizes have been used as a rough guide, but they do not affect the conclusions of our paper; they are based on hydrocode modelling of impacts. Similarly, details of the composition and nature of the Hadean crust and the geotherm, for example, have little effect on our results. This is mainly because our conclusions are based on the effects of large collisions (impactors larger than 100 km); the volumes of melt produced by big impactors are largely insensitive to variation in the mantle potential temperature and its composition. The key factor is the overburden pressure, as detailed above.

We also find that the melt volume increases by ~75% if the mantle potential temperature increases by 200 °C (ref. 70) with respect to the standard case (or 1,600 °C). We also tested the case of a thinner lithosphere (80 km) and found that, for impactors larger than 1,000 km, the volume of melt is generally a few per cent higher than the nominal lithosphere (125 km), and up to 50% higher for impactor sizes between 100 and 1,000 km.

Finally, our estimates of impact-generated melt volume do not consider adiabatic melting of rising mantle elements. The latter process, yet to be the subject of a systematic study, is potentially very important for large projectiles. As discussed in ref. 20, projectiles larger than ~800 km may produce long-lasting perturbations to mantle dynamics. On a short timescale (1–10 Myr relevant for our work), the perturbation is characterized by umbrella-shaped patterns with rising elements at the centre, lateral spreading in the upper mantle and subsequent downwelling (see, for instance, Fig. 7 of ref. 20). As a results, voluminous quantities of rising mantle may melt adiabatically. It is therefore possible that our estimates of the melt production (Fig. 3) are lower bounds, in particular for projectiles larger than 1,000 km.

Concerning the estimate of the final crater size discussed in the text (see, for example, Fig. 2a), we relied on a transient-to-final crater size scaling law derived from lunar craters[71]. Recent work has found that the temperature of the lithosphere has an important role in the modification stage of crater formation[21], and for a hotter target the final crater size can be twice as large as in classical cold scaling. The hot lithosphere scaling is probably more realistic for the early Earth; therefore the final crater sizes discussed here are likely to be underestimated by a factor of ~2.

Impact-generated melt extrusion and Hadean zircon formation. Although it is well-known that zircons can crystallize from impact melt pools (see, for example,

ref. 31), it is argued that the low crystallization temperatures of Hadean zircons are largely incompatible with such an origin[30,31,72]. Our model shows that a fraction of the Earth's uppermost surface layer was melted by impacts. By analogy to recent terrestrial craters (for example Sudbury), it is expected that zircons should have also crystallized from the melt, even for intermediate-to-mafic melts via fractional crystallization[72]. This process would produce zircons that crystallized at higher temperatures than most Hadean zircons[30,73]. Although it is conceivable that a fraction of the high-temperature Hadean zircons ($720\,^{\circ}C < T < 750\,^{\circ}C$) may come from impact melt pools (see, for example, ref. 28), this process seems secondary. Thus, a natural question arises: if impact melt was widespread on the Hadean Earth, why do Hadean zircons have a low crystallization temperature?

Our proposed mechanism naturally explains this observation. We computed the total volume of impact-generated melt produced in a spherical shell 100 km thick (that is, the crust) by all projectiles larger than 50 km. Larger projectiles were assumed not to contribute here because they blast through the shell. The result is that at least 10–20% of the shell is directly melted by impacts. For comparison, we also compute the volume of the shell buried by melt extrusion around the impacts (corresponding to an annulus from 10 to 30 times impactor radii from the impact point, only for projectiles larger than 100 km). This yields >800% of the shell volume, implying that the shell is reprocessed over and over. Therefore the latter process dominates by almost two order of magnitudes with respect to direct impact melt of the shell, explaining the paucity of high crystallization temperature among Hadean zircons. Note that this result is basically independent of the assumed thickness of the shell. A more significant contribution to zircon formation may come from the thick layers of melt extruded onto the surface (Fig. 2b and Extended Data Fig. 5). Given the deep origin of these magmas, however, they were probably ultramafic in composition, thus inhibiting significant zircon formation. Even assuming that low-temperature zircons could have formed from high-temperature melts as a result of fractional crystallization after a substantial decrease in temperature (see, for example, ref. 74), the volume of this fractionated reservoir would have been negligible with respect to the volume of the material buried. Thus the main contribution of these mantle mafic melts was probably as a crustal heat source, not as zircon source material. As discussed in the text, Hadean zircons probably crystallized from wet eutectic melts[3]. Such conditions may have been achieved as a result of impact-generated melt burial of large portions of the surface. In other words, buried weathered material could have been efficiently heated to wet melting conditions by magmatic intrusions (ref. 75, p. 168) from the mantle (as claimed to explain the volcanic plains around the 2,300-km Hellas basin on Mars; refs 19, 25, 76), and by the steepened geotherm produced by thinning of the lithosphere (close to the crater's rims). At larger radial distances, the sinking of lava and crustal recycling (see Fig. 10 of ref. 26; see also a recent commentary in ref. 77) may have been particularly important in a regime characterized by a highly fractured crust (due to impacts), as in the Hadean.

Finally, as discussed in the text, we investigated several impactor fluxes (Extended Data Fig. 2) and how they compare to the Hadean zircon age distribution. The key parameter for this comparison is the ratio of the diameter of the surface melt to the diameter of the projectile (f; see Fig. 3). In the limits of the approximations described above (namely $f \approx 20$–30; see the text), we find that only the nominal case (namely LHB at 4.15 Gyr ago; red curve in Extended Data Fig. 2) reproduces the Hadean zircon age distribution. The case of an LHB at 3.9 Gyr ago fails to reproduce the zircon data for any value of f, whereas the case with no LHB (green curve in Extended Data Fig. 2) only matches the zircon data for $f > 50$. This large f value is unjustified according to our estimates of melt volumes; this scenario is therefore extremely unlikely.

33. Strom, R. G., Malhotra, R., Ito, T., Yoshida, F. & Kring, D. A. The origin of planetary impactors in the inner Solar System. *Science* **309,** 1847–1850 (2005).
34. Marchi, S., Mottola, S., Cremonese, G., Massironi, M. & Martellato, E. A new chronology for the Moon and Mercury. *Astron. J.* **137,** 4936–4948 (2009).
35. Marchi, S., Bottke, W. F., Kring, D. A. & Morbidelli, A. The onset of the lunar cataclysm as recorded in its ancient crater populations. *Earth Planet. Sci. Lett.* **325,** 27–38 (2012).
36. Fassett, C. I., Head, J. W. & Kadish, S. J. *et al.* Lunar impact basins: stratigraphy, sequence and ages from superposed impact crater populations measured from Lunar Orbiter Laser Altimeter (LOLA) data. *J. Geophys. Res. Planets* **117,** E00L08 (2012).
37. Schlichting, H. E., Warren, P. H. & Yin, Q.-Z. The last stages of terrestrial planet formation: dynamical friction and the late veneer. *Astrophys. J.* **752,** 1–8 (2012).
38. Melosh, H. J. *Impact Cratering: A Geologic Process* (Oxford Monographs on Geology and Geophysics no. 11, Clarendon Press, 1989).
39. Murray, C. D. & Dermott, S. F. *Solar System Dynamics* (Cambridge Univ. Press, 1999).
40. Ryder, G. Mass flux in the ancient Earth–Moon system and benign implications for the origin of life on Earth. *J. Geophys. Res. Planets* **107,** E45022 (2002).
41. Norman, M. D. & Nemchin, A. A. A 4.2 billion year old impact basin on the Moon: U–Pb dating of zirconolite and apatite in lunar melt rock 67955. *Earth Planet. Sci. Lett.* **388,** 387–398 (2014).
42. Leinhardt, Z. M. & Stewart, S. T. Collisions between gravity-dominated bodies. I. Outcome regimes and scaling laws. *Astrophys. J.* **745,** 79 (2012).
43. Tonks, W. B. & Melosh, H. J. Core formation by giant impacts. *Icarus* **100,** 326–346 (1992).
44. Kleine, T., Kruijer, T. S. & Sprung, P. in *Lunar and Planetary Science Conf.* 45 2895 (2014).
45. O'Keefe, J. D. & Ahrens, T. J. Planetary cratering mechanics. *J. Geophys. Res.* **98** (E9), 17011–17028 (1993).
46. Holsapple, K. A. The scaling of impact processes in planetary sciences. *Annu. Rev. Earth Planet. Sci.* **21,** 333–373 (1993).
47. Wünnemann, K., Nowka, D., Collins, G. S., Elbeshausen, D. & Bierhaus, M. in Proceedings of 11th Hypervelocity Impact Symposium, 1-13 (2011).
48. Elbeshausen, D., Wünnemann, K. & Collins, G. S. Scaling of oblique impacts in frictional targets: implications for crater size and formation mechanisms. *Icarus* 10.1016/j.icarus.2009.07.018 (2009).
49. Grieve, R. A. F. & Cintala, M. J. An analysis of different impact melt-crater scaling and implications for the terrestrial impact record. *Meteoritics* **27,** 526–538 (1992).
50. Ahrens, T. J. & O'Keefe, J. D. in *Impact and Explosion Cratering* (eds Roddy, D. J., Pepin, R. O. & Merrill, R. B.) 639–656 (Pergamon, 1977).
51. Bjorkman, M. D. & Holsapple, K. A. Velocity scaling impact melt volume. *Int. J. Impact Eng.* **5,** 155–163 (1987).
52. Grieve, R. A., Cintala, M. J. & Therriault, A. M. *Large-scale Impacts and the Evolution of the Earth's Crust: the Early Years* (Geol. Soc. Am. Spec. Pap. 405, 2006).
53. Pierazzo, E., Vickery, A. M. & Melosh, H. J. A reevaluation of impact melt production. *Icarus* **127,** 408–423 (1997).
54. Abramov, O., Wong, S. M. & Kring, D. A. Differential melt scaling for oblique impacts on terrestrial planets. *Icarus* **218,** 906–916 (2012).
55. Ivanov, B. A. & Artemieva, N. A. in *Catastrophic Events and Mass Extinctions: Impact and Beyond* (eds Koeberl, C. & MacLeod, K.) 619–629 (Geol. Soc. Am. Spec. Pap. 356, 2002).
56. Pierazzo, E. & Melosh, H. J. Melt production in oblique impacts. *Icarus* **145,** 252–261 (2000).
57. Chapman, C. R. & McKinnon, W. B. in *Satellites* (eds Burns, J. A. & Matthews, M. S.) 492–580 (Univ. Arizona Press, 1986).
58. Thompson, S. L. & Lauson, H. S. *Improvements in the Chart D Radiation—Hydrodynamic Code 3: Revised Analytic Equation of State* (Sandia Laboratories report SC-RR-71 0714, 1972).
59. Benz, W., Cameron, A. G. W. & Melosh, H. J. The origin of the phase transition (g/cm^3) Moon and the single impact hypothesis. III. *Icarus* **81,** 113–131 (1989).
60. Melosh, H. J. A hydrocode equation of state for SiO_2. *Meteorit. Planet. Sci.* **42,** 2079–2098 (2007).
61. Wünnemann, K., Collins, G. S. & Osinski, G. R. Numerical modelling of impact melt production in porous rocks. *Earth Planet. Sci. Lett.* **269,** 530–539 (2008).
62. Collins, G. S., Melosh, H. J. & Ivanov, B. A. Modeling damage and deformation in impact simulations. *Meteorit. Planet. Sci.* **39,** 217–231 (2004).
63. Melosh, H. J. Acoustic fluidization: a new geologic process? *J. Geophys. Res.* **84,** 7513–7520 (1979).
64. Bierhaus, M., Noack, L., Wuennemann, K. & Breuer, D. in *Lunar and Planetary Science Conf.* 44, 2420 (2013).
65. Stöffler, D. Deformation and transformation of rock-forming minerals by natural and experimental shock processes. I. Behavior of minerals under shock compression. *Fortschr. Mineral.* **49,** 50–113 (1972).
66. Jones, A. P., Wünnemann, K. & Price, D. in *Plates, Plumes, and Paradigms* (eds Foulger, G. R., Natland, J. H., Presnall, D. C. & Anderson, D. L.) 711–720 (Geol. Soc. Am. Spec. Pap. 388, 2005).
67. Huffman, A. R. & Reimold, W. U. Experimental constraints on shock-induced microstructures in naturally deformed silicates. *Tectonophysics* **256,** 165–217 (1996).
68. Schmitt, R. T. Shock experiments with the H6 chondrite Kernouve: pressure calibration of microscopic shock effects. *Meteorit. Planet. Sci.* **35,** 545–560 (2000).
69. Ivanov, B. A. & Melosh, H. J. Impacts do not initiate volcanic eruptions: eruptions close to the crater. *Geology* **31,** 869–872 (2003).
70. Herzberg, C., Condie, K. & Korenaga, J. Thermal history of the Earth and its petrological expression. *Earth Planet. Sci. Lett.* **292,** 79–88 (2010).
71. McKinnon, W. B. & Schenk, P. M. Ejecta blanket scaling on the Moon and Mercury—inferences for projectile populations. *Lunar Planet. Inst. Sci. Conf, Abstr.* **16,** 544–545 (1985).
72. Wielicki, M. M., Harrison, T. M. & Schmitt, A. K. Geochemical signatures and magmatic stability of terrestrial impact produced zircon. *Earth Planet. Sci. Lett.* **321,** 20–31 (2012).
73. Harrison, T. M. & Schmitt, A. K. High sensitivity mapping of Ti distributions in Hadean zircons. *Earth Planet. Sci. Lett.* **261,** 9–19 (2007).
74. Nutman, A. P. Comment on 'Zircon thermometer reveals minimum melting conditions on earliest Earth' II. *Science* **311,** 779 (2006).
75. Turcotte, D. L. & Schubert, G. *Geodynamics* 2nd edn (Cambridge Univ. Press, 2002).
76. Rogers, A. D. & Nazarian, A. H. Evidence for Noachian flood volcanism in Noachis Terra, Mars, and the possible role of Hellas impact basin tectonics. *J. Geophys. Res. Planets* **118,** 1094–1113 (2013).
77. Pearce, J. A. Geochemical fingerprinting of the Earth's oldest rocks. *Geology* **42,** 175–176 (2014).
78. Zahnle, K. *et al.* Emergence of a habitable planet. *Space Sci. Rev.* **129,** 35–78 (2007).
79. Sleep, N. H. The Hadean–Archaean environment. *Cold Spring Harb. Perspect. Biol.* **2,** a002527 (2010).
80. Arndt, N. T. & Nisbet, E. G. Processes on the young Earth and the habitats of early life. *Annu. Rev. Earth Planet. Sci.* **40,** 521–549 (2012).

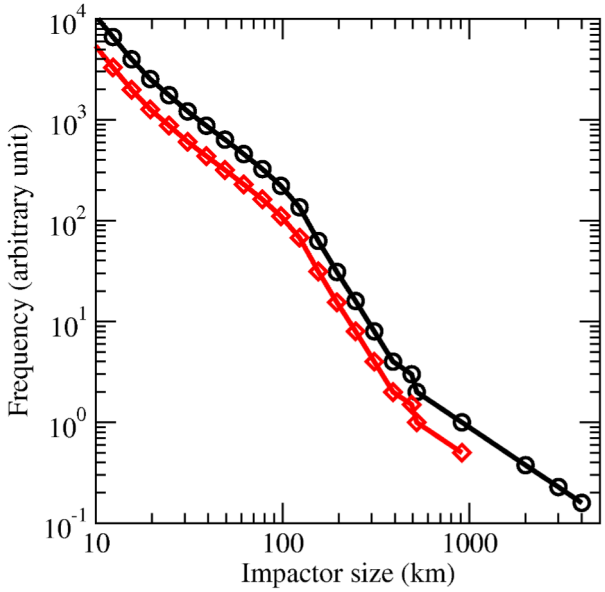

Extended Data Figure 1 | Early Earth's impactor size–frequency distributions. The red curve corresponds to current main-belt asteroids larger than 10 km. The largest object is Ceres, whose diameter is ~913 km. The black curve (vertically shifted for clarity) is a replicate of the main-belt curve, extrapolated to 4,000 km by using the slope in the size range 500–913 km.

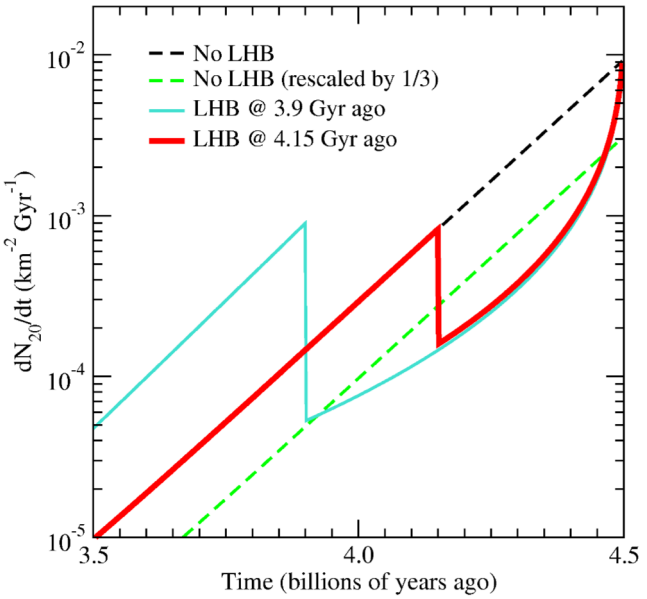

Extended Data Figure 2 | Lunar impact fluxes. The differential number of lunar craters >20 km (N_{20}) as a function of time and per unit surface for several scenarios discussed in the text.

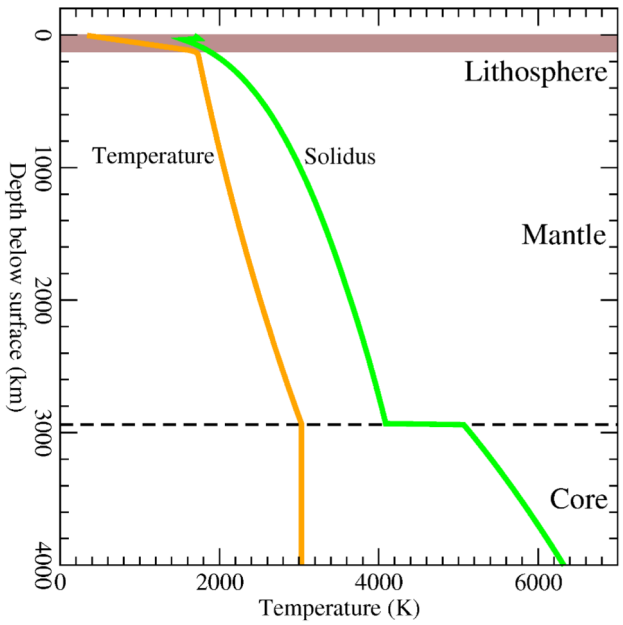

Extended Data Figure 3 | Solidus and geotherm used in iSALE simulations. Note the temperature increase in the lithosphere that results in an increase in the temperature of buried surface material. Other processes resulting in an increase of the temperature of the buried crust are discussed in the text. The assumed thermal gradient is a lower limit (see Extended Data Table 1), implying that the increase in the temperature of the buried material can be significantly higher than is shown here.

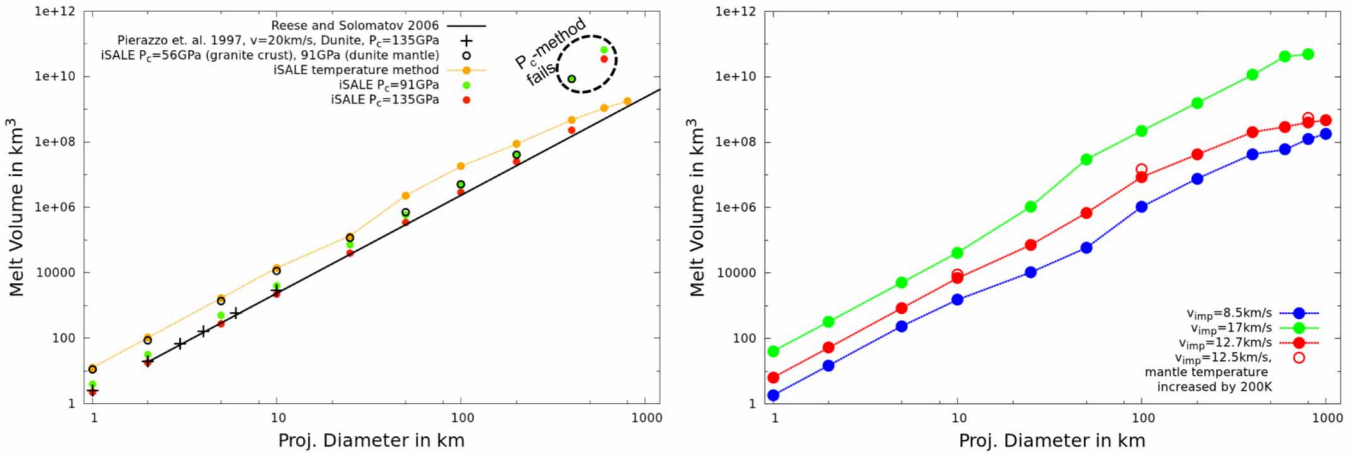

Extended Data Figure 4 | Impact-generated melt volume. Left, comparison of melt volume production for various methods; right, comparison of melt volume production for various impact velocities and mantle potential temperature (see the text for more details).

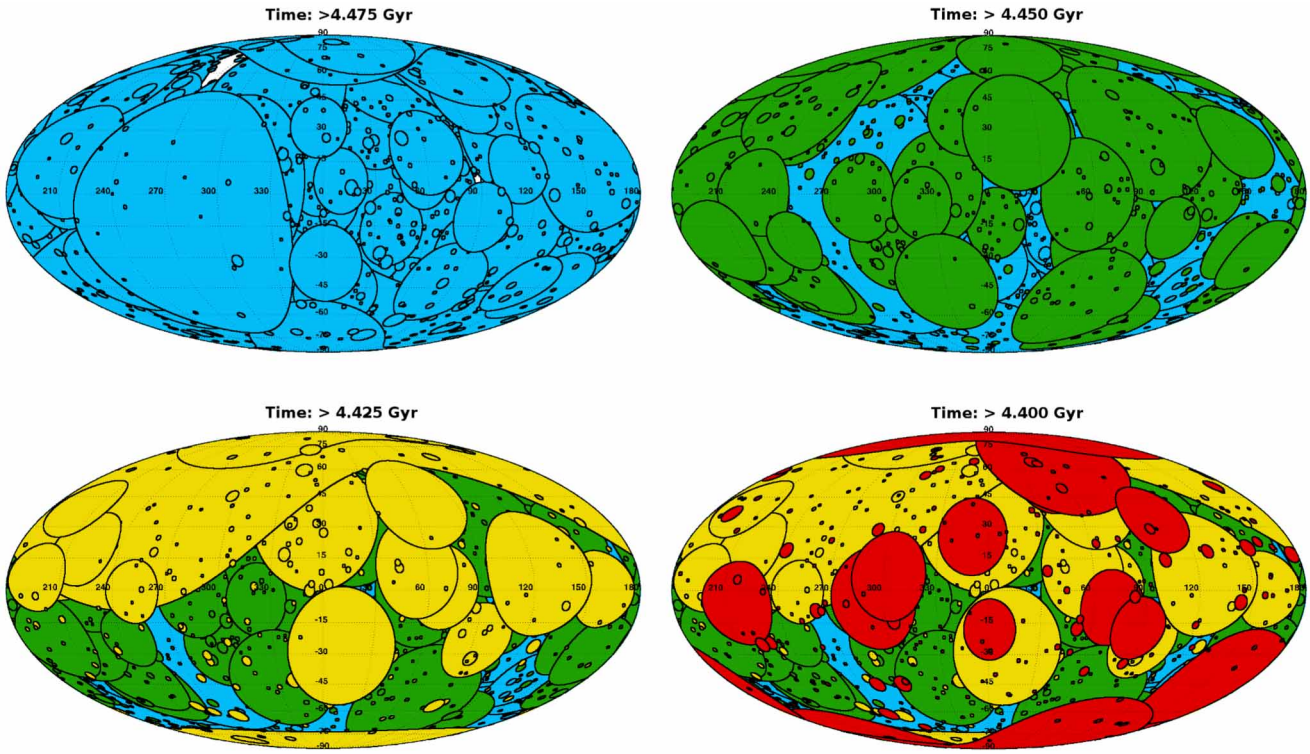

Extended Data Figure 5 | Melt spreading over the first 100 Myr of Earth history. Mollweide projections of the cumulative record of craters at four different times. There are portions of the Earth's surface that are not affected by impact-generated melt at each time step, except for the first 25 Myr (or >4.475 Gyr). However, there is no significant fraction of the Earth's surface that is unaffected by impacts before ~4 Gyr ago (see also Fig. 2b). Impacts therefore set the stage for the environmental conditions on the Hadean Earth and have implications for the origin and development of life (see, for instance, discussion in refs 78–80).

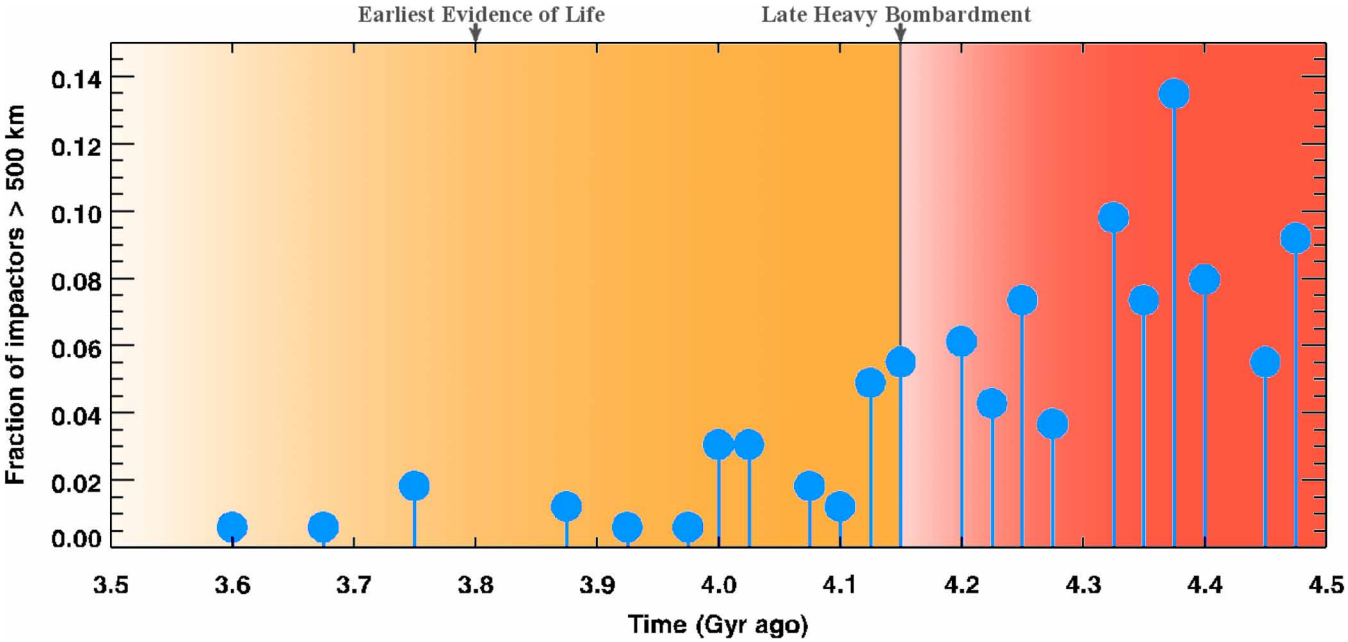

Extended Data Figure 6 | Minimum impact time for projectiles larger than 500 km. Blue dots indicate the minimum impact time for impactors larger than 500 km recorded in 163 successful Monte Carlo simulations (see Fig. 1). The vertical axis reports the number of impacts (in bins of 25 Myr each) normalized by the number of simulations. The lowest *y* values shown in the plot correspond to one impact. The median time is 4.32 Gyr ago, and the mean is 4.27 Gyr ago. The earliest evidence of life on Earth (~3.8 Gyr ago), and the start of the Late Heavy bombardment (~4.15 Gyr ago; see the text) are also indicated. About 10% of the simulations have a minimum time of 4 Gyr ago or less.

Extended Data Table 1 | Various parameters used for iSALE simulations

Model parameters	
Cells per projectile radius (CPPR)	50
Gravity (m/s^2)	9.81
Crustal thickness (km)	30
Mantle thickness (km)	2900
Impact velocity (km/s)	8.5;12.7;17.0
Impactor size (km)	1-4000
Surface temperature (°C)	20
Lithospheric temperature gradient (°C/km)	11.25
Lithosphere thickness (km)	125
Planet radius (km)	6371
Core temperature (°C)	2727

Material parameters	granite	dunite	iron
Melt temperature at zero pressure (°C)	1400	1100	1538
Heat capacity (J/(kg*K))	1000.0	1000.0	600.0
Constant Simon approximation for solidus (Pa)*	6.00E+9	1.52E+9	6.0E+9
Exponent in Simon approximation for solidus*	3.0	4.05	3.0
Cohesion of damaged material (Pa)	1.0E+4	1.0E+4	1.0E+4
Cohesion of intact material (Pa)	1.0E+7	1.0E+7	-
Coefficient of friction for intact material	0.6	0.6	0.4
Coefficient of friction for damaged material	2.0	1.2	-

Note that our results on impact-generated melt for large impactors are fairly insensitive to the assumed lithospheric geotherm gradient because most of the melt is produced at depth. Here we adopted a conservative low value. For additional discussion on the effects of geotherm see ref. 69.
* For the definition of these parameters, see ref. 69.